Precise optical control of gene expression in *C. elegans* using genetic code expansion and Cre recombinase

Lloyd Davis[1], Inja Radman[2,3], Angeliki Goutou[1,3], Ailish Tynan[1], Kieran Baxter[1], Zhiyan Xi[1], Jack M. O'Shea[1], Jason W. Chin[2]* & Sebastian Greiss[1]*

[1] Centre for Discovery Brain Sciences, University of Edinburgh, UK
[2] Medical Research Council Laboratory of Molecular Biology, Cambridge, UK
[3] These authors contributed equally
* email: s.greiss@ed.ac.uk; chin@mrc-lmb.cam.ac.uk

Abstract

Synthetic strategies for optically controlling gene expression may enable the precise spatiotemporal control of genes in any combination of cells that cannot be targeted with specific promoters. We develop an efficient genetic code expansion system in *C. elegans* and use it to create a photo-activatable Cre recombinase. We laser-activate Cre in single neurons within a bilaterally symmetric pair to selectively switch on expression of a loxP controlled optogenetic channel in the targeted neuron. We use the system to dissect, in freely moving animals, the individual contributions of the mechanosensory neurons PLML/PLMR to the *C. elegans* touch response circuit, revealing distinct and synergistic roles for these neurons. We thus demonstrate how genetic code expansion and optical targeting can be combined to break the symmetry of neuron pairs and dissect behavioural outputs of individual neurons that cannot be genetically targeted.

Introduction

Genetic code expansion offers the ability to introduce, during translation, functionalities into proteins beyond those offered by the set of canonical, naturally occurring amino acids. This is achieved by providing orthogonal translation components: an orthogonal aminoacyl-tRNA synthetase (aaRS) paired with a cognate orthogonal tRNA, and assignment of a codon to determine the site of incorporation of a non-canonical amino acid (ncAA) (Chin 2017). Currently available orthogonal systems, however, often lack the efficiency required to fully harness the possibilities offered by genetic code expansion, especially in multicellular systems. A large variety of non-canonical amino acids are available for *in vivo* use, among them photocaged amino acids, which can be used to confer light activated control over the function of proteins in a host organism (Courtney and Deiters 2018).

Sequence specific DNA recombinases, such as Cre and FLP, have become transformative for controlling gene expression in many systems, including worms, flies, and vertebrates, by irreversibly activating or deactivating target gene expression. Indeed, the photo-induced reconstitution of split recombinases (Schindler et al. 2015; Kawano et al. 2016) might be used to optically target recombinase activity to a single cell. However, the sensitivity of this technique can be hampered by high background levels of light-independent recombinase activity.

Moreover, these systems are induced using blue light, rendering their use incompatible with most optogenetic and imaging applications, and requiring cells to be kept in the dark, complicating their use in transparent model systems. Recently, genetic code expansion methods were used to create photocaged versions of Cre in cultured mammalian cells and zebrafish embryos (Luo et al. 2016; Brown et al. 2018). In photocaged Cre, an orthogonal aaRS / $tRNA_{CUA}$ pair is used to replace a catalytically critical tyrosine or lysine residue in the active site of Cre with a photocaged tyrosine or lysine residue, resulting in a catalytically inactive enzyme (Luo et al. 2016; Brown et al. 2018). The photocaging group can then be removed through a short exposure to 365 nm UV light, activating Cre recombinase, which in turn activates expression of its target genes. We set out to create an optimised photocaged Cre system that enables the optical activation of gene expression in single cells in an animal. The precise spatiotemporal control of gene expression offered by photocaged Cre, would have a wide range of applications by allowing the expression of genes of interest in single cells or combinations of cells. Applied to control, for example, optogenetic channels or other neuromodulatory proteins, it could be a transformative tool in neurobiology.

Defining the molecular and cellular basis of behaviour is a fundamental challenge in neuroscience. *C. elegans* contains 302 neurons, for which the physical connectivity has been determined (White et al. 1986). This physical map provides a conceptual framework within which to design experiments to understand the signal processing properties of neural circuits that define behaviour. Central to this endeavour are methods for the spatiotemporal control of gene expression that enable precise perturbations to be effected in individual cells or combinations of cells and thereby advance our understanding of cellular contributions to circuit function. Two thirds of the neurons in *C. elegans* exist in bilaterally symmetric (left and right) pairs, and similar gross morphological symmetries are seen in the nervous systems of many other animals. A central question is whether and how this morphological symmetry is broken to produce functional asymmetry (Troemel, Sagasti, and Bargmann 1999; Wes and Bargmann 2001; Suzuki et al. 2008; Hobert, Johnston, and Chang 2002).

Tissue specific promoters (alone or in combination) can be used to target groups of cells. However, this approach offers only limited precision, and in many cases appropriate promoters are unavailable; especially in scenarios when investigators aim to limit expression to a single cell or a defined subset of cells. This is particularly limiting in neuroscience studies where the goal is to couple neuronal activity of single neurons or a defined subset of neurons with functional output. Where specific promoters for targeting individual neurons are unavailable, laser ablation can be used to remove specific neurons, but this technology is not compatible with studying intact circuits. Optogenetic approaches using targeted illumination have been applied to stimulate groups or pairs of cells, and track resulting behavioral outputs in freely moving *C. elegans* (Leifer et al. 2011; Stirman et al. 2011; Kocabas et al. 2012). However, without a means of precisely defining expression of optogenetic tools, this approach is technically very challenging as it requires specialized software and hardware tools for real-time tracking and targeting and does not lend itself to isolating single cells in neuronal pairs. Similar obstacles are encountered in other systems, where the solution often also requires technically challenging approaches utilising targeted illumination (Chen, Papagiakoumou, and Emiliani 2018).

Here we describe the optimisation of genetic code expansion for ncAA incorporation and the optimisation of a photocaged Cre recombinase variant (optPC-Cre) in *C. elegans*. The combination of these advances allows us to optically control gene expression with unprecedented precision and over 95% efficiency in a population of animals (compared to less than 1% efficiency before optimization). By using a microscope mounted 365 nm laser, we photo-activate Cre and thereby control gene expression in single cells (**Figure 1**). We name this approach **Laser Targeted Activation of Cre-Lox recombination** (LaserTAC). LaserTAC is fast and within the technical capabilities of any lab currently able to perform laser ablation, allowing easy generation, in a single session, of dozens of animals with defined expression patterns for use in downstream experiments. We demonstrate the utility of LaserTAC by using it to target the expression of optogenetic channels to individual *C. elegans* touch sensory neurons within a left/right pair (PLML and PLMR). These individual neurons cannot be targeted by other methods, and our approach allows us to study their contribution to behaviour for the first time. Our results reveal that the PLM neurons act in synergy to produce a robust touch response requiring input from both neurons. Furthermore, the individual neurons within this pair make asymmetric contributions to the touch response, suggesting distinct roles for PLMR and PLML in the habituation to repeated stimulation.

115
116

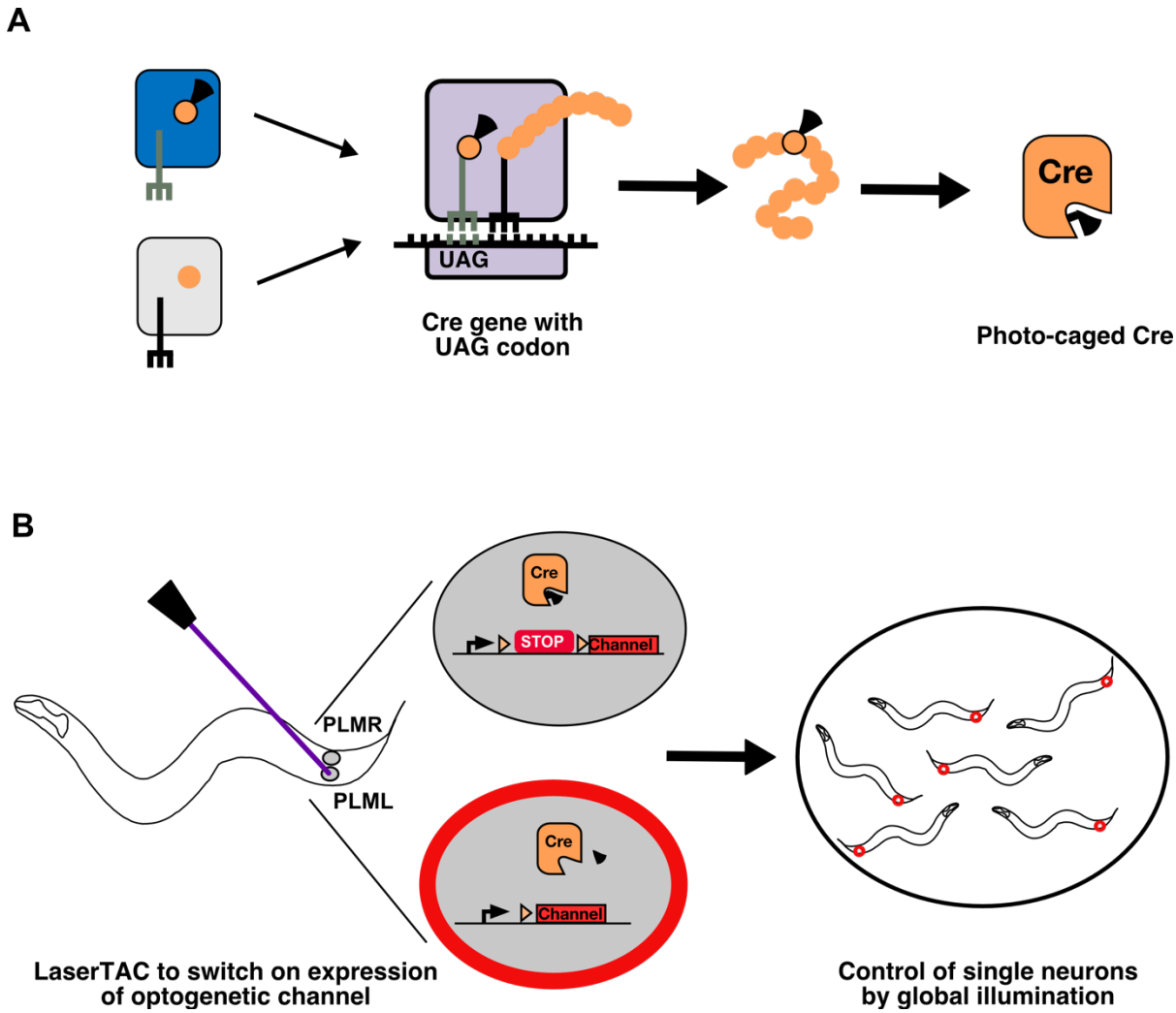

117
118
119 **Figure 1. Genetic code expansion and LaserTAC**. **(A)** A non-canonical amino acid, e.g. photocaged lysine
120 (PCK), is charged onto the orthogonal $tRNA_{CUA}$ by the orthogonal aminoacyl-tRNA synthetase (top left). The
121 orthogonal components do not interact with the native cellular amino acids, tRNAs, or tRNA-synthetases (bottom
122 left). After charging, PCK is incorporated into the expanding polypeptide chain in response to an amber stop codon
123 (UAG) during ribosomal translation. The resultant polypeptide is released following translation resulting in full-
124 length photocaged Cre containing the PCK residue. **(B)** Photocaged Cre recombinase is activated cell-specifically
125 in single *C. elegans* neurons by uncaging the PCK in its active site using a 365 nm laser. Activated Cre switches
126 on expression of an optogenetic channel. Global illumination of freely moving animals can then be used to control
127 cells expressing the optogenetic channel.
128

Results

Improved ncAA incorporation

Efficient genetic code expansion depends on the ability of the orthogonal aminoacyl-tRNA synthetase to aminoacylate its cognate $tRNA_{CUA}$, which in turn delivers the ncAA to the ribosome for incorporation in response to the UAG amber stop codon (**Figure 1A**). The charging of the ncAA onto the $tRNA_{CUA}$ occurs mainly in the cytoplasm, and efficient charging is therefore dependent on cytoplasmic aminoacyl-tRNA synthetase availability.

The orthogonal pyrrolysyl-tRNA synthetase (PylRS) / tRNA(Pyl) pair from archeal *Methanosarcina species* is the most versatile and widely used pair for genetic code expansion (Wan, Tharp, and Liu 2014; Brown, Liu, and Deiters 2018). The PylRS / tRNA(Pyl) pair is functional in *C. elegans*, and variants exist that recognise photocaged amino acids (Greiss and Chin 2011; Gautier et al. 2010).

When expressed in eukaryotic cells, PylRS is localised predominantly to the nucleus due to a stretch of positively charged amino acids in the N-terminal domain, which is interpreted as a nuclear localisation sequence by the eukaryotic nuclear import machinery. Accordingly, addition of a rationally designed strong nuclear export sequence (S-NES) to the PylRS N-terminus was reported to significantly increase the efficiency of ncAA incorporation in mammalian cells by increasing the amount of cytoplasmic PylRS (Nikić et al. 2016).

To test this approach in *C. elegans,* we added the reported S-NES sequence to the N-terminus of PCKRS, a PylRS variant optimised for incorporating photocaged lysine (PCK) (Gautier et al. 2010) (**Figure 2A**). We used the ubiquitous *C. elegans* promoter *sur-5p* (Yochem, Gu, and Han 1998) to drive S-NES::PCKRS expression and *rpr-1p* (Parrish et al. 2012) to drive $tRNA(Pyl)_{CUA}$ expression. To assay PCK incorporation efficiency we used a dual colour incorporation sensor; a ubiquitously expressed GFP::mCherry fusion, with the two fluorophore coding sequences separated by an amber stop codon (Greiss and Chin 2011) (**Figure 2B**). For this reporter, translation in the absence of PCK leads to termination at the amber stop codon resulting in production of only GFP. Conversely, in the presence of PCK, $tRNA(Pyl)_{CUA}$ is charged with the ncAA and acts as a nonsense suppressor, resulting in production of the full-length GFP::mCherry fusion protein, which includes a nuclear localisation sequence and an HA tag at its C-terminus. However, we did not detect any significant difference in incorporation between worms expressing unmodified PCKRS and S-NES::PCKRS. In fact, incorporation levels when using the S-NES::PCKRS construct appeared to be lower than with unmodified PCKRS (constructs "no NES" & "S-NES" **Figure 2C, figure supplement 1A**).

To test whether S-NES::PCKRS and unmodified PCKRS localise as predicted, we expressed S-NES::PCKRS::GFP and PCKRS::GFP fusion proteins. As expected, the S-NES::PCKRS::GFP fusion localised to the cytoplasm, while unmodified PCKRS::GFP was almost entirely nuclear, reflecting that the S-NES was able to efficiently shift PCKRS localisation from the nucleus to the cytoplasm (constructs "no NES" & "S-NES" **Figure 2D, figure supplement 1B**). Therefore, we hypothesised that the S-NES tag itself might impinge on PCK incorporation efficiency. We next performed a mini-screen of three nuclear export sequences from human proteins: p120cts-NES, PKIα-NES, and Smad4-NES, which are demonstrated to act as NESs in *C. elegans* (Yumerefendi et al. 2015). All tested NES sequences achieved nuclear export of the synthetase PCKRS (**Figure 2D – figure supplement 1B**).

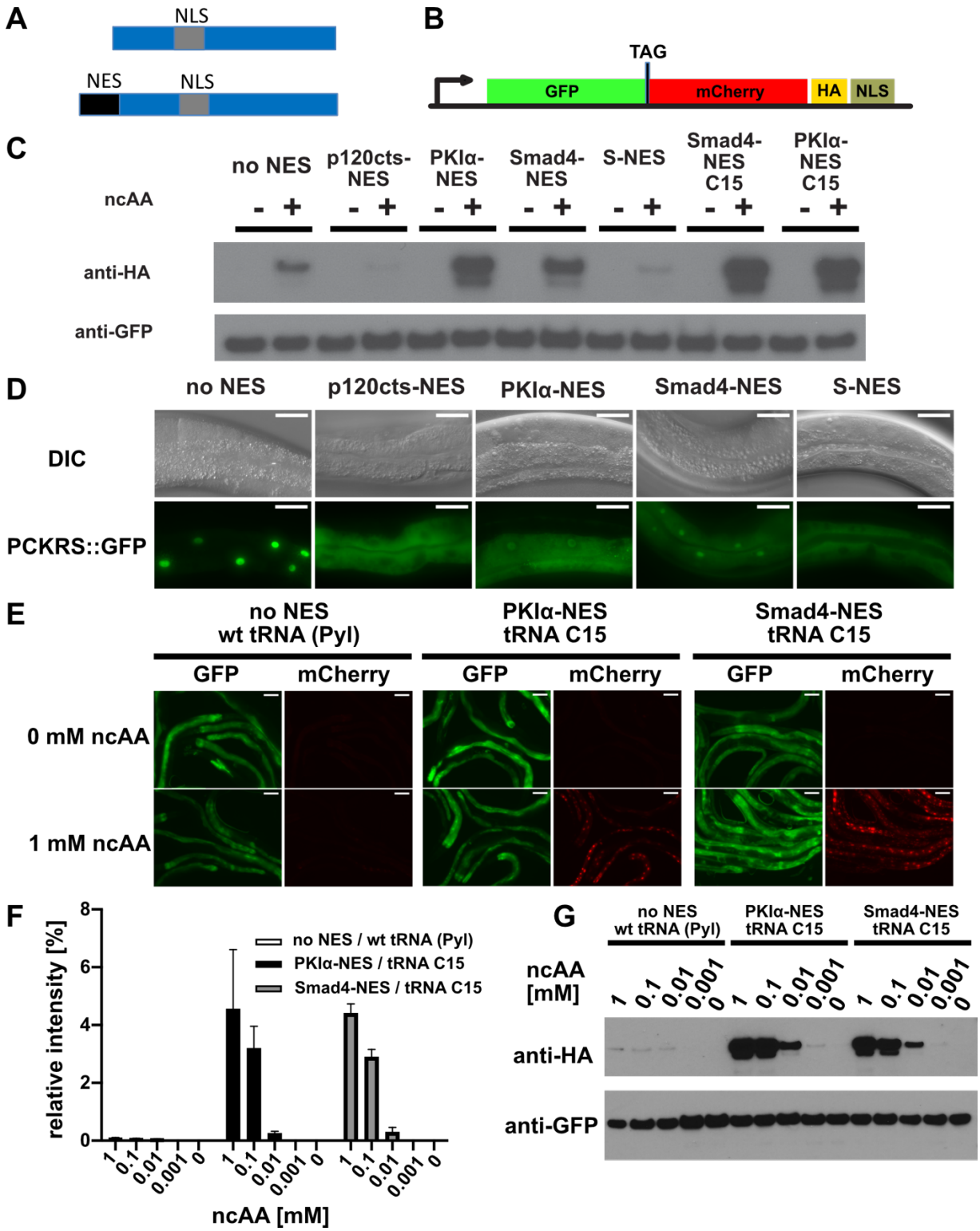

Figure 2. Efficiency of genetic code expansion is enhanced in *C. elegans* by use of NES::PCKRS variants and tRNA(C15). (**A**) wild type PylRS/PCKRS (top) contains an internal nuclear localization sequence (NLS) which targets it to the nucleus. A strong nuclear export sequence (NES) can be added to PylRS/PCKRS to shift it to the cytoplasm (bottom). (**B**) The GFP::mCherry reporter has an intersubunit linker containing an amber stop codon (TAG) to direct incorporation of ncAA. The C-terminal NLS moves full length product to the nucleus, providing a second visual readout, whilst the C-terminal HA tag provides a target for Western blotting of full-length protein. (**C**) Western blot (anti-HA) for full-length reporter produced using PCKRS with different NES attached to the N-terminus. For comparison the wild type PCKRS without NES and the two best NES variants together with optimised tRNA(C15) are also shown. + or – indicates the respective presence or absence of 1mM ncAA. Samples were normalised using anti-GFP. Quantitative western blots of the lines used are shown in figure supplement 1A. (**D**) Nuclear localization of NES variants fused to PCKRS. Localization visualized by imaging of a GFP protein

directly fused to each NES::PCKRS variant. scale bars 30 μm. Nuclear to cytoplasmic ratios for the wild type PCKRS::GFP fusion and two independent lines for each NES variant are shown in figure supplement 1B (**E**) Fluorescent images of randomly selected worms grown in the presence or absence of 1mM ncAA. GFP indicates expression of reporter construct, mCherry indicates presence of full-length reporter protein. Scale bars 80 μm. Enlarged versions of the images for PKIa-NES and Smad4-NES are shown in figure supplement 1C (**F**) Quantification of Western blots of wild type PCKRS ("no NES") / tRNA(Pyl) vs both PKIα-NES::PCKRS / tRNA(C15) and Smad4-NES::PCKRS / tRNA(C15) at different ncAA concentrations; anti-GFP was used to detect both the full length GFP;;mCherry prtein as well as the GFP truncated at the amber stop. The graphs show the relative intensities of the full length GFP signal vs the signal of the GFP truncated at the amber stop codon. Graphs represent the average of 2 lines and 3 independent experiments per condition, each experiment was blotted twice. **(G)** conditions shown in (F) probed with anti-HA and anti-GFP. In (G) only one line was blotted for each condition.

However, the NES variants differentially affected incorporation efficiencies: when we co-expressed NES::PCKRS variants with tRNA(Pyl) and the GFP::mCherry incorporation reporter, we found that the p120cts-NES variant reduced incorporation efficiency below the level of unmodified PCKRS, whereas the PKIα-NES and the Smad4-NES robustly increased PCK incorporation efficiency (**Figure 2C – Figure supplement 1A**). We selected the two most efficient PCKRS variants for subsequent optimisation experiments.

We then turned to the optimisation of tRNA(Pyl). tRNA(Pyl) contains secondary structure elements not present in canonical mammalian tRNAs. These features reduce compatibility with the endogenous translational machinery. which limits ncAA incorporation in mammalian cells. However, ncAA incorporation efficiency in cultured mammalian cells can be improved by introducing mammalian tRNA elements into the archaeal tRNA(Pyl), or by using engineered mitochondrial tRNAs (Serfling et al. 2018). To investigate whether the same approach might improve ncAA incorporation efficiency in other eukaryotes, we tested an improved tRNA variant in the *C. elegans* system. Specifically, we co-expressed the mitochondrial tRNA based variant C15, previously validated in mammalian cells (Serfling et al. 2018) together with the GFP::mCherry incorporation reporter, and the two most efficient synthetase variants described above (namely Smad4-NES::PCKRS or PKIα-NES::PCKRS). We found that the presence of the C15 variant significantly increased incorporation efficiency (**Figure 2C, E, F, G, figure supplement 1A,C).** Compared to the unmodified PCKRS / tRNA(Pyl) pair, the Smad4-NES::PCKRS / tRNA(C15) and PKIα-NES::PCKRS / tRNA(C15) pairs improved incorporation efficiency by more than 50-fold; from < 0.1% to 4.6% and 4.4% respectively (**Figure 2F**). We performed all further experiments using the Smad4-NES::PCKRS / tRNA(C15) pair.

Expression of photocaged Cre recombinase

We next applied our improved incorporation system to express photocaged Cre recombinase (PC-Cre) in the N2 wild type *C. elegans* laboratory strain. Cre recombinase can be photocaged by replacing K201, a lysine residue in the Cre active site, critical for enzyme activity, with photocaged lysine (PCK) (Gibb et al. 2010; Luo et al. 2016) (**Figure 3A, B**). PC-Cre has previously been expressed in both mammalian cell culture and zebrafish embryos using transient transfection and direct mRNA/tRNA injections (Luo et al. 2016; Brown et al. 2018). To direct incorporation of PCK, we generated a PC-Cre construct where we replaced the lysine codon at position 201 in the Cre sequence with an amber stop codon (TAG). The PC-Cre construct was expressed in an artificial operon with GFP, allowing us to visualise its expression. We used as a Cre recombinase target gene a fluorescently tagged

channelrhodopsin ChR2::mKate2, separated from its promoter by a transcriptional terminator flanked by loxP sites (**Figure 3C**).

We generated transgenic animals containing all genetic components: the optimized orthogonal synthetase / tRNA pair Smad4-NES::PCKRS / tRNA(C15), the PC-Cre construct and the floxed Cre target ChR2::mKate2. All protein coding components were driven by a *glr-1p* promoter, an ortholog of human GRIA1 (glutamate ionotropic receptor AMPA type subunit 1). This promoter is active in glutamatergic neurons, including command interneurons (Maricq et al. 1995) (**Figure 3 - figure supplement 1A**). We grew animals on PCK from the L1 larval stage and activated PC-Cre by UV illumination when they had reached the L4 larval stage (after two days). 24h after activation, we saw strong expression of ChR2::mKate2 in neurons expressing PC-Cre. In contrast, we saw no expression of ChR2::mKate2 in animals which had undergone UV illumination without prior feeding on PCK, and in animals fed on PCK but which had not undergone UV illumination (**Figure 3 - figure supplement 1B**). Furthermore, as expected for a membrane channel, the red fluorescence of ChR2::mKate2 was localised at the cellular membrane. We observed red fluorescence only in cells expressing the *glr-1p* promoter, as evidenced by overlap with *glr-1p* driven expression of GFP.

Using the optimised Smad4-NES::PCKRS / tRNA(C15) expression system, we observed expression of the target locus, indicative of PC-Cre photo-activation, in 63% of animals 24h after uncaging. We saw no red fluorescence without UV treatment. The 63% activation rate was a vast improvement relative to the 1% we observed with unmodified PCKRS and tRNA(Pyl) (**Figure 3D**).

Improving photocaged Cre Recombinase

To further improve the photo-activation method we next turned to PC-Cre optimisation. When using amber stop codons for ncAA incorporation, the $tRNA_{CUA}$ competes with endogenous release factors. This competition results in a mixture of full-length polypeptides, with ncAA incorporated, as well as truncated polypeptides due to translational termination at the amber stop codon. As assessed with the GFP::mCherry incorporation reporter, we show that the percentage of full-length protein is between 4% - 5% when using the improved Smad4-NES::PCKRS / tRNA(C15) incorporation system (**Figure 2F**). It is likely that, similar to the fluorescent reporter, the majority of translation events of the PC-Cre mRNA will also terminate at the internal amber stop codon, even in the presence of PCK. A Cre protein truncated at the amber stop codon in position 201 is missing the majority of its active site, but the parts of Cre responsible for the protein-protein interaction required for active Cre tetramer formation are still present, as are large parts of the DNA binding interface (Guo, Gopaul, and van Duyne 1997). We initially based PC-Cre on previously reported Cre constructs, which contain an N-terminal SV40 NLS in addition to the internal NLS native to Cre (Luo et al. 2016; Brown et al. 2018; Le et al. 1999; Macosko et al. 2009), thus ensuring localisation of the enzyme to the nucleus. We cannot exclude the possibility that truncated Cre, which locates to the nucleus due to the NLSs upstream of position 201, may interfere with tetramer formation or DNA binding.

We aimed to utilise the *C. elegans* nuclear import machinery to enrich for full-length product in the nucleus. Since Cre acts on nuclear DNA, we reasoned that we could boost PC-Cre activity by lowering the fraction of truncated PC-Cre while increasing the fraction of full-length PC-Cre present in the nucleus. To this end, we

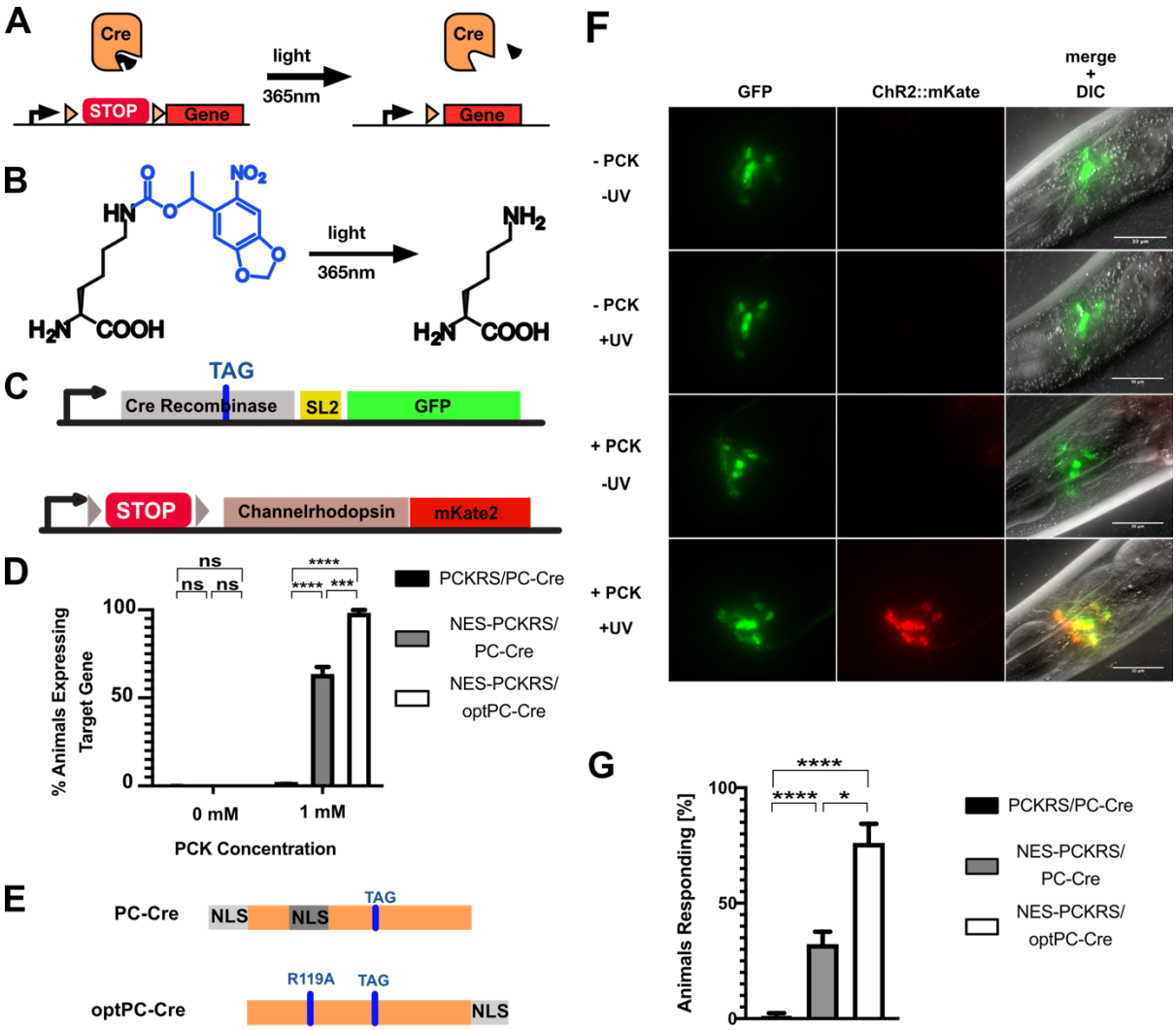

Figure 3. Optimisation of PC-Cre recombinase for genetic code expansion in *C. elegans*. (**A**) Cre recombinase can by photocaged by incorporating a photocaged ncAA into the active site (black wedge). Transcription of a target gene is blocked by placing a transcription terminator sequence ("STOP") between the gene and its promoter. The terminator sequence is flanked by loxP sites (orange triangles). Upon illumination at 365 nm the photocaging group is removed and the uncaged, active Cre removes the transcriptional terminator. (**B**) 6-nitropiperonyl-L-Lysine, "photocaged lysine" (PCK) is a lysine residue with a 2-nitrobenzyl derived photocaging group on the side chain. The photocaging group is removed at 365 nm. (**C**) Genetic constructs for PC-Cre controlled expression of channelrhodopsin. See also figure supplement 1A (**D**) Cre activation efficiency in animals with optimised vs original constructs. Comparison of original PCKRS and tRNA(Pyl)$_{CUA}$ ("PCKRS"), Smad4-NES::PCKRS and tRNA(C15) ("NES-PCKRS"), original photocaged Cre recombinase ("PC-Cre") and optimized photocaged Cre ("optPC-Cre"). Three experiments were performed using two independent lines for each condition. In each experiment 30 animals were visually scored for ChR2::mKate2 expression for each condition. Significance determined by Welch's t test. The error is the SEM (n=6). (**E**) Schematic showing PC-Cre and optPC-Cre. Substitution mutations shown as blue bars. The TAG mutation denotes the site of PCK incorporation. PC-Cre contains both an N-terminal and internal NLS. OptPC-Cre contains only a C-terminal NLS, the R119A mutation disables the internal NLS. (**F**) Imaging of worms expressing Smad4-NES::PCKRS, tRNA(C15) and optPC-Cre. Expression of ChR2::mKate2 is dependent on supplementation of PCK and uncaging by exposure to UV light. Scale bars 30μm (**G**) Percentage of animals reversing in response to a blue light pulse. "PCKRS": original PCKRS and tRNA(Pyl)$_{CUA}$; "NES-PCKRS": Smad4-NES::PCKRS and tRNA(C15); "PC-Cre": original photocaged Cre recombinase; "optPC-Cre": optimized photocaged Cre. Assays were carried out using two independent lines and > 10 animals for each genotype, the mean of three stimulations was determined. The graph shows the mean of two experiments. Significance obtained by Mann-Whitney U test. The error is the SEM (n=4). *p<0.05, ***p<0.001, ****p<0.0001

removed both NLSs upstream of position 201 by introducing a R119A mutation disabling the internal NLS sequence (Le et al. 1999) and by removing the N-terminal SV40 NLS. To restore nuclear import for full length PC-Cre only, we attached the strong *C. elegans* EGL-13 NLS (Lyssenko, Hanna-Rose, and Schlegel 2007) to the Cre C-terminus to create optimised PC-Cre (optPC-Cre) **(Figure 3E)**. When we compared optPC-Cre to PC-Cre, we indeed found that target gene activation was significantly improved: from 63% for PC-Cre to 97% for optPC-Cre (**Figure 3D**). We saw no expression of the ChR2::mKate2 target gene without PCK or UV activation **(Figure 3D, F).**

We next performed behavioural assays to assess whether our system allowed optical control of neurons. After activation of optPC-Cre, we waited 24h to achieve sufficient expression of ChR2::mKate2, which we confirmed by visual inspection under a dissecting fluorescence microscope. When we exposed worms to 470 nm blue light to activate ChR2, we observed clear reversals in worms expressing ChR2::mKate2 in the presence of the ChR2 cofactor all-trans retinal (ATR). In animals expressing ChR2::mKate2 in the absence of ATR we did not observe such reactions **(Figure 3G, figure supplement 1C, Videos 1,2)**. The induced behaviour concurs with previous studies showing that optogenetic activation of neurons expressing ChR2 from the *glr-1p* promoter induces backward movement (Schultheis et al. 2011). When we compared strains expressing PC-Cre and optPC-Cre respectively, we saw the strongest and most robust responses in the strains where optPC-Cre was used to control expression of ChR2::mKate2, followed by strains using non optimised PC-Cre, but using the efficient Smad4-NES::PCKRS / tRNA(C15) incorporation system. Animals expressing unmodified PCKRS and non-optimised Cre showed almost no response to optogenetic activation (**Figure 3G, figure supplement 1C**). Taken together, we conclude that optPC-Cre is an effective tool with which to control optogenetic channel expression for the purpose of optical control of neuronal activity.

Cell-specific gene activation using LaserTAC

The use of light to control activity of Cre recombinase should allow precise spatial control of Cre-dependent DNA recombination. We tested the precision of uncaging by using a microscope mounted 365 nm laser to target individual cells in the touch response circuitry. *C. elegans* has six mechanosensory neurons for the perception of soft touch: AVM, ALML and ALMR, which are located in the anterior of the worm, and PVM, PLML and PLMR, which are located in the posterior (**Figure 4A**). Activation of the touch receptor neurons results in avoidance behaviour. Worms respond with backward movement to an anterior touch, and with forward movement to a posterior touch (Chalfie et al. 1985). Previous studies using targeted ChR2 illumination in individual animals likewise showed that optogenetic activation of the anterior neurons AVM and ALM results in reversals, while activation of the posterior neurons PVM and PLM results in forward movement. Concurrent activation of all 6 neurons results in reversals in the majority of cases. Repeated activation leads to a reduced response due to habituation (Leifer et al. 2011; Stirman et al. 2011; Schild and Glauser 2015).

We aimed to investigate the posterior PLM neurons by using LaserTAC to selectively express the optogenetic channel Chrimson (Schild and Glauser 2015) in both PLM neurons, or in PLML and PLMR individually. To this end, we generated strains with Smad-4-NES::PCKRS and optPC-Cre expression driven by the *mec-7p* promoter, which is active in all six mechanosensory neurons (Mitani et al. 1993). To

express Chrimson, we used a Chrimson::mKate2 fusion gene separated from the pan-neuronal *maco-1p* promoter by a transcriptional terminator flanked by loxP sites (Figure 4 - **figure supplement 1A**). We chose the panneuronal *maco-1p* promoter, an orthologue of human MACO1 (macoilin 1) (Arellano-Carbajal et al. 2011), because in contrast to *mec-7p*, it shows increasing expression from the L4 larval to the adult stage, the age when we aimed to induce Chrimson::mKate2 expression (**Figure 4 - figure supplement 1B**).

To activate expression of the Chrimson channel in the PLM neurons, we mounted age-synchronised L4 stage animals, grown on PCK from L1, on a microscope slide and used a Micropoint Galvo system to deliver a short 2-4 second 365 nm pulse to individual cells, targeting the nucleus. After uncaging, we transferred the worms to an NGM agar plate without PCK for recovery and to allow for induced Chrimson::mKate2 expression (**Figure 4B**). After 12-24h, we observed Chrimson::mKate2 expression that was only present in laser-targeted cells. We were able to selectively activate optPC-Cre in both PLM neurons, as well as in PLML or PLMR alone (**Figure 4C-E**).

We confirmed that the presence of the PCK incorporation machinery and optPC-Cre did not affect the function of the touch sensory neurons by assaying the animals response to soft touch (Chalfie et al. 2014) (**Figure 4 - figure supplement 1C,D**).

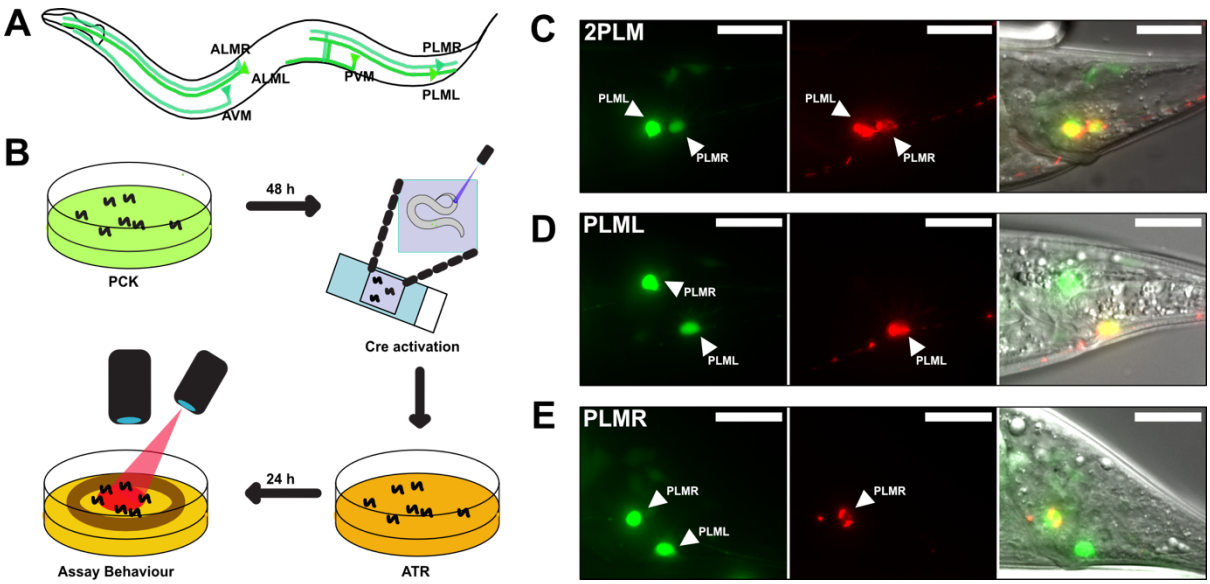

Figure 4. LaserTAC using optimised photocaged Cre-recombinase facilitates cell-specific expression of optogenetic channels in *C. elegans*. (A) Map of the six *C. elegans* touch receptor neurons showing the posterior location of the PLM neuron pair. **(B)** Diagram of experimental procedure for activating expression of target genes in single cells using LaserTAC, followed by optogenetic behavioural assay. **(E, F, G)** Fluorescent images showing targeted expression of Chrimson::mKate2 24h after laser induced activation of optPC-Cre (middle panels) in both PLM neurons (E), only in PLML (F), only in PLMR (G). Scale bars 20μm. GFP signal in the left panels indicates cells expressing optPC-Cre.

Optogenetic manipulation of PLM touch sensory neurons reveals distinct and synergistic roles for PLML and PLMR in the soft touch response

To determine the behavioural response to PLM stimulation, we prepared animals expressing Chrimson::mKate2 in either both PLM neurons, or in PLML or PLMR alone. After optPC-Cre activation we grew the worms on plates supplemented with ATR for 24h to allow expression of the optogenetic channel and confirmed the desired expression pattern under a fluorescence dissecting microscope.

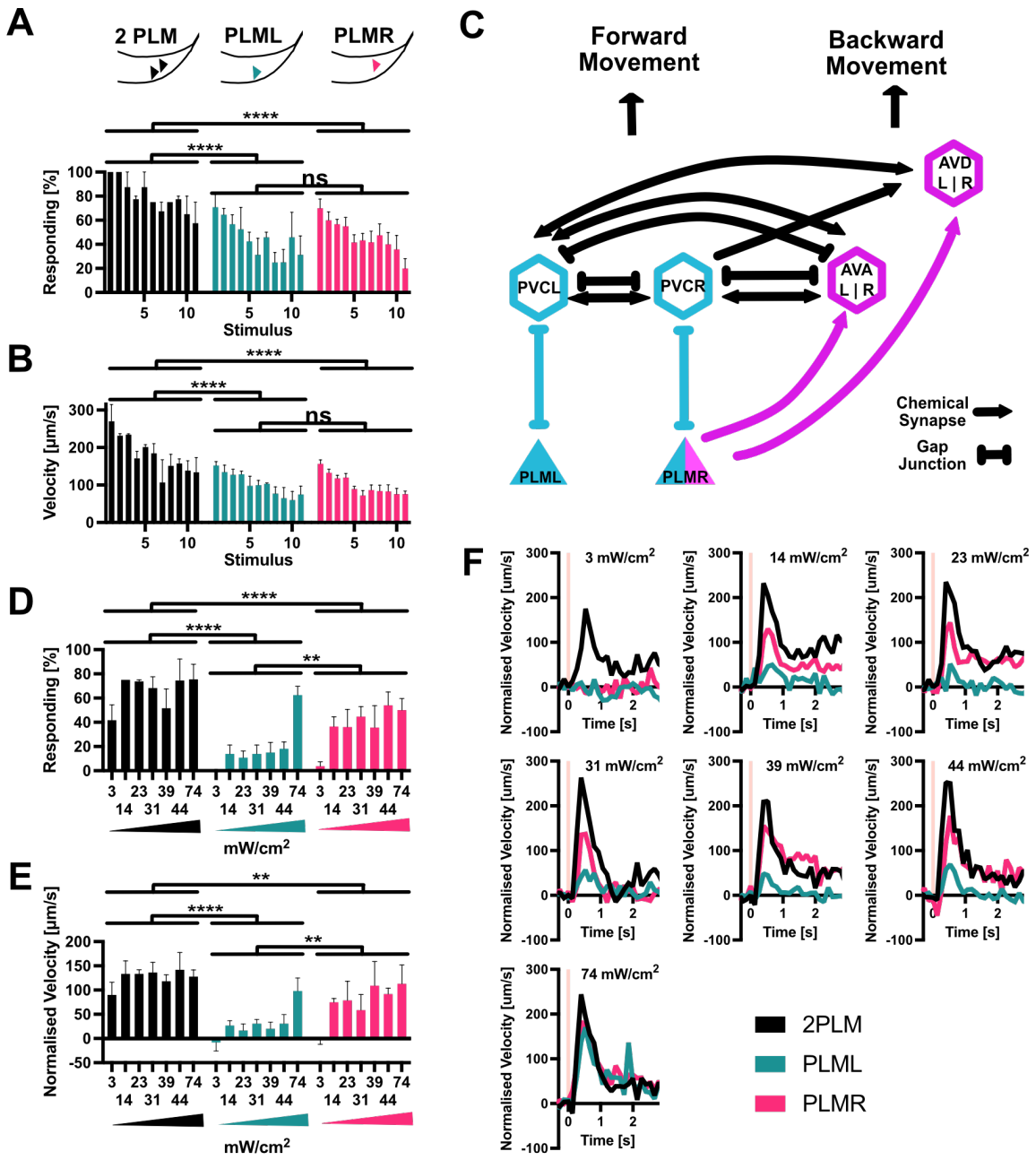

Figure 5 PLM neurons show distinct responses to optogenetic stimulation. (A) Percentage of animals responding to repeated stimulations with light pulses of 1s, 74 mW/cm², 617 nm, delivered every 30s. Worms expressed Chrimson in either both PLM neurons ("2PLM", black), only in PLML (blue-green), or only in PLMR (red). Responding worms are defined as those having mean forward speeds greater than 100µms^{-1} over the 2s following stimulation. Assays were performed with cohorts of 4 to 6 worms stimulated simultaneously, one cohort constitutes a replicate. Replicates were assayed on different days. Significances derived from 2-way ANOVA (2PLM n=2; PLML and PLMR n=4). **(B)** Mean velocity for the experiments analysed in (A). Mean velocity was determined for each cohort. Significances derived from 2-way ANOVA. (2PLM n=2; PLML and PLMR n=4) **(C)** Simplified schematic of the asymmetric neuronal connectivity of PLML and PLMR within the touch circuit. Symmetric PLM connections are shown in light blue whereas asymmetric connections shown in magenta. **(D)** Percentages of animals which respond to stimulation (0.1s, 617 nm) at the power levels indicated. Chrimson expressed in either both PLM neurons ("2PLM", black), only in PLML (blue-green) or only in PLMR (red). For each individual worm the velocity was measured in the 1s window from 0.2s to 1.2s after stimulation, which corresponds to the peak response. Velocities were then normalised by subtracting the average speed of the individual over the 0.5s immediately prior to stimulation. Responding worms are defined as those having mean normalised forward speeds greater than 100µm/s in the 1s window from 0.2s to 1.2s after stimulation. Cohorts of 4 to 8 animals were stimulated together and the mean velocity of one cohort constitutes a replicate. Replicates were assayed on different days. Significances derived from 2-way ANOVA, n=3 for all conditions **(E)** Mean normalised velocity for the experiments analysed in (D). The mean normalised velocity across all animals within a

cohort was determined for the 1s window 0.2s to 1.2s after stimulation. Significances derived from 2-way ANOVA. n=3 for all conditions **(F)** Normalised mean velocity traces of the experiments analysed for (D,E) across all 3 replicates for each condition at the power levels indicated. 2PLM (black), PLML (blue-green) and PLMR (red). Pink vertical lines indicate the light pulse. Traces before normalisation are shown in figure supplement 2.

We then activated Chrimson::mKate2 expressing neurons by illumination for 1s every 30s with 617 nm at the maximum power setting of 74 mW/cm^2. During the assay the animals were moving freely on the plate and we illuminated the entire plate. We found that illumination of animals expressing Chrimson::mKate2 in both PLM neurons ("2PLM") triggered a robust response with the worms initiating forward movement (**Figure 5A, B – figure supplement 1, Video 3**). Conversely, mock-treated animals ("0PLM"), grown on PCK and ATR but without activation of optPC-Cre showed no response (**Figure 5 - figure supplement 1**, **Video 4**). Animals expressing Chrimson::mKate2 only in the PLML or the PLMR neurons respectively also showed a clear reaction to stimulation (**Figure 5A, B, figure supplement 1, Videos 5, 6**). For all three expression patterns (2PLM, PLML, PLMR) we observed a gradual reduction in the response with increasing number of stimulations, both in the fraction of animals responding and in the speed upon stimulation, consistent with habituation to the stimulus (Stirman et al. 2011). We found that the 2PLM animals responded stronger to stimulation than animals expressing Chrimson::mKate2 in either PLML or PLMR alone, both in regard to the fraction of animals responding, and by velocity (**Figure 5A, B**).

We then proceeded to more closely investigate the responses to activation of PLML and PLMR individually. The members of the PLM neuron pair, PLML and PLMR, show a striking asymmetry in their connections within the worm connectome (**Figure 5C**) (Chalfie et al. 1985). PLMR forms chemical synapses connecting it to 10 downstream neurons including the AVA and AVD interneuron pairs, which are involved in driving backward locomotion. In addition to chemical synapses, PLMR also forms gap junctions to PVCR, PHCR and LUAR. PLML on the other hand is connected to the touch response circuit exclusively through gap junctions, formed with the interneurons PVCL, PHCL and LUAL. In fact, PLML does not form any chemical synapses, with the exception of a single connection to HSNL, a neuron involved in the control of egg laying. Asymmetric wiring of PLML and PLMR has been proposed to influence the *C. elegans* tap response, a withdrawal reflex that integrates information from the anterior and posterior mechanosensory neurons. In worms with ablation of both PLM neurons and the single PLMR neuron, a tap stimulus increased backward movement. In contrast, ablating PLML had no effect (Wicks and Rankin 1995).

As we saw no difference between PLML and PLMR in the response to strong stimulation (Figure 5A,B), we decided to test the animals' responses to weaker stimulation of the PLM neurons. For this, we reduced the duration of the 617 nm light pulse from 1s to 0.1s and delivered varying low intensities, starting at 3 mW/cm^2, the lowest setting that was possible with our set up. While the 0.1s, 3 mW/cm^2 stimulus was sufficient to elicit a response in animals expressing Chrimson in both PLMs, neither PLML or PLMR animals reacted, indicating a synergistic effect of PLML and PLMR and the requirement for activation of both neurons to elicit a reaction in response to weak stimuli (**Figure 5D-F – figure supplement 2**).

When we increased illumination intensity, we saw a striking difference appear between the responses to PLML and PLMR stimulation respectively. Animals

465 expressing Chrimson in PLMR showed a robust reaction to stimulation at 14 mW/cm^2
466 and higher. In contrast, the response of PLML animals was consistently below that
467 of PLMR or 2PLM animals (**Figure 5D-F – figure supplement 2**). Only at the highest
468 intensity setting of 74 mW/cm^2 did we observe animals of all three expression
469 patterns responding robustly to the stimulus. The observed differences in response
470 for PLML and PLMR are not due to differential expression of Chrimson::mKate2
471 (**Figure 5 - figure supplement 3**), therefore they are likely due to the asymmetric
472 connectivity of the two neurons within the *C. elegans* nervous system.
473

474 ## Discussion

475 We demonstrate a robust, improved method for highly efficient ncAA
476 incorporation in *C. elegans*. Our optimised ncAA incorporation system will provide
477 the means to introduce a wide range of new chemical functionalities into proteins,
478 such as crosslinkers, biorthogonal groups, and post translational modifications, and
479 serve as a catalyst for new approaches to manipulate and understand cellular biology
480 in *C elegans* (Chin 2017; Davis and Chin 2012; Nguyen, Cigler, and Lang 2018; Lang
481 and Chin 2014; Young and Schultz 2018; Zhang et al. 2015; Baker and Deiters 2014).
482 Furthermore, since our optimisation approach is based on components that are not
483 specific to *C. elegans*, we expect that it will be easily exportable to other organisms.
484 The genetic code expansion approach relies on the use of an amber stop codon
485 to direct incorporation of ncAA, which means that endogenous TAG codons may be
486 inadvertently suppressed by the orthogonal system, albeit likely at low levels.
487 Interestingly, *C. elegans* and other organisms have evolved natural surveillance
488 mechanisms to mitigate against the read-through of stop codons (Arribere et al.
489 2016), which will also mitigate against any potential effects caused by our system.
490 Indeed, we find that the function of the mechanosensory neurons we assay is
491 unaffected by the presence of the orthogonal ncAA incorporation machinery.
492 We demonstrate the utility of our system by creating LaserTAC, which is based
493 on an optimised photo-activatable Cre recombinase and offers several unique
494 advantages for optical control of gene expression. First, the recombinase activity is
495 tightly controlled; the presence of the photocaging group completely blocks activity
496 and upon photo-activation, highly efficient wild type Cre is generated. Second,
497 following photo-activation, the photocaged amino acid required for amber stop
498 codon suppression can be removed. Thus translation of full length Cre ceases,
499 leaving worms devoid of photocaged Cre for subsequent biological studies
500 (Maywood et al. 2018). Third, due to the stability of the photocaging group at longer
501 wavelengths, our photo-activatable Cre is fully compatible with imaging and
502 optogenetic methods that use visible light.
503 We used LaserTAC to switch on optogenetic channel expression in individual
504 neurons within a bilaterally symmetric pair that cannot be targeted by genetic means.
505 Switching on gene expression using LaserTAC is fast, and easily enables the
506 preparation of dozens of animals for downstream experiments. Light activation
507 requires only a microscope-mounted laser, generally used for ablation in most *C.*
508 *elegans* laboratories, modified to emit light at 365 nm. Generating the required
509 transgenic strains is straightforward and at present involves the introduction of the
510 genetic constructs, followed by genomic integration. The power of the method we
511 present here lies in the versatility it offers, not only in respect to the ability to
512 investigate single neurons. Once a transgenic strain is made, any combination of

513 neurons targeted by the promoter that was used can in principle be investigated. This
514 removes the requirement for the creation of a potentially large numbers of lines, by
515 allowing multiple conditions to be investigated using a single strain. A further
516 advantage offered by or approach is the ability of precise temporal control, which is
517 generally not available using promoter based systems.
518 We demonstrate the capabilities of LaserTAC by targeting expression of the
519 optogenetic channel Chrimson to the mechanosensory PLM neurons. This enables
520 us to analyse, the individual contributions of the neurons PLML and PLMR to the *C.*
521 *elegans* tail touch circuit response. Since we target expression of the optogenetic
522 channel, we can perform behavioural assays by globally illuminating a plate of freely
523 moving animals.
524 We found that PLML and PLMR show some redundancy in triggering the tail touch
525 response after strong stimulation. However, using weaker stimuli, we found that only
526 stimulation of both neurons elicits a response, indicative of a synergistic rather than
527 a simply redundant role for PLML and PLMR. Interestingly, our results demonstrate
528 asymmetric contributions of PLML and PLMR to the touch response. Considering the
529 electrical and chemical connectome of this circuit (**Figure 5C**), our results are
530 consistent with a model where the touch response is controlled by two parallel
531 pathways that rely on gap junctions or chemical synapses respectively. The first
532 pathway involves direct connections of both PLM neurons to the PVC interneurons
533 via gap junctions. Activation of the PVCs through these gap junctions triggers forward
534 motion. The PVCs form connections with forward command interneuron AVB as well
535 as inhibitory connections with backward command interneurons AVA/AVD. The
536 second pathway involves chemical synaptic transmission from PLMR onto AVA &
537 AVD, inhibiting backward locomotion. Thus, when only PLMR is stimulated, both
538 pathways are activated, resulting in a stronger response, whereas when PLML alone
539 is stimulated only the gap junction pathway is activated, resulting in a weaker
540 response. Unlike the PLMs, the PVCs are connected to each other by gap junctions
541 and may thus act as electrical sinks for signals from the PLMs. This could help to
542 explain the requirement for stronger stimulation of the single neurons, especially for
543 PLML, to trigger a response as compared to the stimulation of both PLMs
544 simultaneously. Stimulation of both PLM neurons together results in full activation of
545 the gap junction pathway by activating both PVC neurons, which together with the
546 direct inhibition of AVA/AVD by PLMR, results in full activation of the tail touch motor
547 response. The strong synergistic effect we observe with the simultaneous stimulation
548 of PLML and PLMR indicates a requirement for the stimulation of both PVC neurons.
549 While we focused here on expression of optogenetic channels in *C. elegans*
550 neurons, simple extensions of our method will enable the cell-specific expression of
551 other desired transgenes of interest. By inserting loxP sites into genomic loci using
552 CRISPR/Cas9, it should be possible to control, at single cell resolution, the
553 expression of any endogenous protein, such as neuropeptides, receptors, innexins,
554 proteins involved in synaptic transmission, etc. Since the components we employ are
555 functional in other *C. elegans* tissues (Greiss and Chin 2011) and indeed in other
556 model systems such as zebrafish, fruit fly, mouse, cultured cells and *ex vivo* tissues,
557 we anticipate that our method will have broad applicability beyond the nervous
558 system and beyond *C. elegans*.
559

Materials & Methods

Plasmids

All expression plasmids were generated from pENTR plasmids using Gateway cloning. All plasmids are described in Supplementary Table 1.

C. elegans strains

Strains were maintained under standard conditions unless otherwise indicated (Brenner 1974; Stiernagle 2006).

Transgenic worms were generated by biolistic bombardment using hygromycin B as a selection marker (Radman, Greiss, and Chin 2013; Davis and Greiss 2018) in either N2 or *smg-2(e2008)* genetic background. The *smg-2(e2008)* background lacks a functional nonsense mediated decay machinery and was used to increase levels of reporter mRNA (Greiss and Chin 2011). Gamma-irradiation to generate the integrated line SGR56 from SGR55 was carried out by Michael Fasseas (Invermis / Magnitude Biosciences). After integration the line was backcrossed into N2 and subsequently maintained on standard NGM without added hygromycinB. SGR56 was backcrossed twice, SGR96 was backcrossed 4 times. All non-integrated lines were maintained on NGM supplemented with hygromycin B (0.3 mg/ml) (Formedium). Strains used in this paper are listed in Supplementary Table 2.

Imaging and image analysis

All imaging was carried out on a Zeiss M2 imager. Worms were mounted on glass slides for imaging and immobilised in a drop of M9 supplemented with 25mM NaN_3.

Fluorescent images were analysed using ImageJ software. To determine nuclear to cytoplasmic ratios of NES::PCKRS::GFP variants, mean fluorescence intensity was measured for a region of interest within the nucleus and divided by the mean intensity of a region in the cytoplasm proximal to the nucleus. To compare Chrimson::mKate2 levels in the PLML and PLMR neurons, the threshold function was used to create regions of interest encompassing the neurons and the mean intensity of those regions was taken.

ncAA feeding

Photocaged lysine (PCK) (Gautier et al. 2010) was custom synthesised by ChiroBlock GmbH, Germany. PCK-NGM plates were prepared by dissolving PCK powder in a small volume of 0.02M HCl and adding the solution to molten NGM. The HCl in the NGM was neutralised by addition of equimolar amounts of NaOH as previously described (Davis and Greiss 2018).

Animals were age synchronised by bleaching (Stiernagle 2006) and added to PCK-NGM plates as L1 larvae. Food was then added to the PCK-NGM plates in the form of solubilised freeze-dried OP50 (LabTIE) reconstituted according to the manufacturer's instructions.

Worm Lysis and Western blotting

Synchronised populations were grown on PCK-NGM plates until the young adult stage and washed off plates using M9 buffer supplemented with 0.001% Triton-X100. Worms were settled, supernatant was removed and worms were resuspended in undiluted 4xLDS loading buffer (ThermoFisher) supplemented with NuPAGE Sample

608 Reducing Agent (ThermoFisher). Lysis was performed by a freeze/thaw cycle
609 followed by 10 min incubation at 95ºC.
610 Samples were run on precast Bolt 4 to 12% gels (ThermoFisher) for 19 min at
611 200V. Proteins were transferred from the gel onto a nitrocellulose membrane using
612 an iBlot2 device (ThermoFisher).
613 After transfer, the membrane was blocked using 5% milk powder in PBST (PBS +
614 0.1% Tween-20) for 1h at room temperature. Incubation with primary antibodies was
615 carried out in PBST + 5% milk powder at 4ºC overnight. Blots were washed 6 x 5
616 minutes with PBST + 5% milk powder before incubating with secondary antibody for
617 1h at room temperature.
618 Antibodies used are listed in Supplementary Table 2. Pierce ECL Western Blotting
619 Substrate (Thermo Scientific) or SuperSignal West Femto chemiluminescent
620 Substrate (Thermo Scientific) were used as detection agent. For quantitative blots, a
621 C-DiGit Blot Scanner (LI-COR) was used, intensities were analysed using
622 ImageStudio software.
623
624 **Global uncaging of PCK for Cre activation**
625 Worms were age synchronised and grown on PCK-NGM plates for 48h, washed
626 onto unseeded 6cm NGM plates and illuminated for 5 min, 5mW/cm^2 in a 365 nm CL-
627 1000L crosslinker (UVP) as previously described (Davis and Greiss 2018). After
628 uncaging, worms were transferred to seeded NGM plates and scored for expression
629 of the target gene 24 h later, by counting the animals showing expression of the red
630 fluorescent marker. 400 μM FUDR was added to plates after uncaging to prevent
631 hatching of F1 progeny and thus aid scoring of animals expressing the target gene
632 All plates were scored twice, independently by two people. Scoring was performed
633 blind. Experiments were performed three times, each with two independent
634 transgenic lines. Significance tests were carried out using Welch's t test as a pairwise
635 comparison between each condition at each concentration using GraphPad Prism8
636 software.
637
638 **Uncaging for Cre activation in single neurons**
639 Worms were grown on 4mM PCK from the L1 stage. For uncaging, worms were
640 mounted on a 3% agar and immobilised with 25mM NaN_3 in M9 buffer. Targeting was
641 performed on a Zeiss M2 Imager using a Micropoint Galvo module (Andor Technology
642 / Oxford Instruments), fitted with a 365 nm dye cell. Neurons were identified using
643 GFP as a guide, which was co-expressed with photocaged Cre, and the nucleus
644 targeted with the laser. Each region was swept thrice using 10 repeat firing. The
645 manual attenuator was set to full power and the Andor software attenuator to a power
646 of 34 (we chose the power setting so that partial bleaching of GFP could be observed
647 during Micropoint firing). After uncaging, the coverslip was removed and worms were
648 washed off the pad onto seeded 6cm plates using M9 + 0.001% Triton-X. Mock laser
649 treatment control worms were mounted and recovered similar to experimental worms
650 but without exposure to the Micropoint laser.
651
652 **Behavioural Assays**
653 Immediately after uncaging, worms were transferred to NGM plates
654 supplemented with ATR (30μl 5mM ATR dissolved in ethanol were added to the lawn

of a seeded 6cm NGM plate) or control NGM only plates. Worms were left to recover on plates for 24 hours after uncaging.

Plates for behavioural assays were made approximately one hour before use. Fresh 6cm NGM plates were seeded with a 20μl drop of dilute OP50, prepared from freeze dried OP50 (LabTIE). For this, the freeze-dried bacteria were reconstituted according to the manufacturer's instructions and a 40x dilution of the reconstituted bacteria was used to spot the plates. The lawn was then surrounded by a copper ring (inner diameter 17 mm) to prevent worms from leaving the camera field of view. For experiments on PLM, expression of the target gene after optPC-Cre laser activation was visually confirmed using a Leica M165FC fluorescence microscope fitted with a 2.0x objective and animals showing the correct pattern (either both neurons or individual neurons, depending on the uncaging experiment) were picked onto the behaviour plates. For experiments using the *glr-1p* promoter, animals were randomly picked. After transfer, worms were left to acclimatise on behaviour plates for at least 10 minutes. Behavioural assays were carried out using a WormLab system (MBF Bioscience). Chrimson or Channelrhodopsin2 were activated using either the integrated 617 nm LED or 470 nm LED of the WormLab platform at 74mW/cm^2 or 150mW/cm^2 respectively, unless otherwise stated.

Tracking of worm behaviour was carried out using WormLab software (MBF Bioscience). For each worm, tracks detected by the WormLab software were consolidated into a single track. Data points where individual animals were not clearly identified by the software were discarded.

For all behavioural experiments, worms were grouped into cohorts. A cohort consisted of 4 to 10 animals undergoing the same treatment simultaneously on the same plate.

Behavioural experiments on worms expressing ChR2 from the *glr-1p* promoter were carried out by exposing worms to 1s of 470 nm illumination at 150mW/cm^2. Reversals were counted manually. The reversal percentages were determined for each replicate. Significance between conditions was tested using a Mann-Whitney U test.

Experiments using repeated stimulation of animals expressing Chrimson::mKate2 in the PLM neurons were carried out by exposing worms to repeated 1s long stimulations with 617 nm light (74 mW/cm^2) at 30s intervals. Raw speed data was binned and averaged at 1s intervals for each animal. Worms were grouped by cohort. To determine the fraction of animals responding to a stimulus, worms with an average speed ≥ 100 μms^{-1} in the 2s following stimulation were scored as responders. The 100 μms^{-1} threshold was selected as it constitutes the standard deviation of the mean speed of unstimulated worms. For each time point, the percentage of worms responding was determined for each cohort, constituting one replicate. Comparison between conditions was carried out by 2-way ANOVA across all stimuli.

Experiments comparing conditions across different power levels for animals expressing Chrimson::mKate2 in the PLM neurons were carried out by subjecting each cohort of worms to 0.1s stimulation with 617 nm at the indicated power levels. The percentage of worms responding for each cohort was calculated after first normalising the data by subtracting the mean speed for each individual worm in the 0.5s immediately prior to stimulation. Then the mean velocity for each individual worm was determined for the response peak between 0.2s and 1.2s after

stimulation. Worms were scored as responders if the mean normalised velocity was ≥ 100 μms^{-1}.
When calculating the mean normalised velocity across experiments, the mean velocity among all animals within a cohort was determined first, followed by calculating the average of the mean velocities across cohorts. Significance for both analyses (fraction responding/intensity and mean velocity/intensity) was determined by 2-way ANOVA.

Analysis and Statistics

All statistical analysis of data was carried out in GraphPad Prism 8. Statistical tests are stated in figure legends.

All values of n in this manuscript, unless otherwise stated, refer to biological replicates. For behavioural experiments we define as biological replicates cohorts of worms that were assayed on different days. A cohort of worms consisted of animals undergoing treatment and assayed together on the same plate.

Acknowledgements:

We thank Maria Doitsidou, Netta Cohen, Kathrin Lang, Emanuel Busch, and Bill Schafer for helpful suggestions and input on the manuscript, and Zoltan Soltesz for help with initial experiments.

We thank the European Research Council (ERC-StG-679990), the Wellcome-Trust University of Edinburgh Institutional Strategic Support Fund ISS2, the Royal Society, and the Muir Maxwell Epilepsy Centre for funding to S.G., the University of Edinburgh for a Edinburgh Global Award and Principal's Career Development PhD studentship to Z.X.; we thank the MRC (MC_U105181009 and MC_UP_A024_1008) and the Louis Jeantet Foundation for funding to J.W.C.; I.R. thanks the Herchel Smith Foundation for a studentship.

Some strains were provided by the Caenorhabditis Genetics Centre for strains, funded by NIH Office of Research Infrastructure Programs (P40OD010440).

References

Arellano-Carbajal, Fausto, Luis Briseño-Roa, Africa Couto, Benny H.H. Cheung, Michel Labouesse, and Mario de Bono. 2011. "Macoilin, a Conserved Nervous System-Specific ER Membrane Protein That Regulates Neuronal Excitability." *PLoS Genetics* 7 (3). https://doi.org/10.1371/journal.pgen.1001341.

Arribere, Joshua A, Elif S Cenik, Nimit Jain, Gaelen T Hess, Cameron H Lee, Michael C Bassik, and Andrew Z Fire. 2016. "Translation Readthrough Mitigation." *Nature*, June, 1–17. http://dx.doi.org/10.1038/nature18308.

Baker, Austin S., and Alexander Deiters. 2014. "Optical Control of Protein Function through Unnatural Amino Acid Mutagenesis and Other Optogenetic Approaches." *ACS Chemical Biology* 9 (7): 1398–1407. https://doi.org/10.1021/cb500176x.

Brenner, S. 1974. "The Genetics of *Caenorhabditis elegans*." *Genetics* 77 (1): 71–94.

Brown, Wes, Jihe Liu, and Alexander Deiters. 2018. "Genetic Code Expansion in Animals." *ACS Chemical Biology* 13 (9): 2375–86. https://pubs.acs.org/doi/pdf/10.1021/acschembio.8b00520.

Brown, Wes, Jihe Liu, Michael Tsang, and Alexander Deiters. 2018. "Cell-Lineage Tracing in Zebrafish Embryos with an Expanded Genetic Code." *Chembiochem : A European Journal of Chemical Biology* 19 (12): 1244–49. http://doi.wiley.com/10.1002/cbic.201800040.

Chalfie, M, J E Sulston, J G White, E Southgate, J N Thomson, and S Brenner. 1985. "The Neural Circuit for Touch Sensitivity in *Caenorhabditis elegans*." *The Journal of Neuroscience : The Official Journal of the Society for Neuroscience* 5 (4): 956–64.

Chalfie, Martin, Anne C. Hart, Catharine H. Rankin, and Miriam B. Goodman. 2014. "Assaying Mechanosensation." *WormBook : The Online Review of C. elegans Biology*, 1–13. https://doi.org/10.1895/wormbook.1.172.1.

Chen, I. Wen, Eirini Papagiakoumou, and Valentina Emiliani. 2018. "Towards Circuit Optogenetics." *Current Opinion in Neurobiology* 50: 179–89. https://doi.org/10.1016/j.conb.2018.03.008.

Chin, Jason W. 2017. "Expanding and Reprogramming the Genetic Code." *Nature* 550 (7674): 53–60. http://dx.doi.org/10.1038/nature24031.

Courtney, Taylor, and Alexander Deiters. 2018. "Recent Advances in the Optical Control of Protein Function through Genetic Code Expansion." *Current Opinion in Chemical Biology* 46: 99–107. https://doi.org/10.1016/j.cbpa.2018.07.011.

Davis, Lloyd, and Jason W Chin. 2012. "Designer Proteins: Applications of Genetic Code Expansion in Cell Biology." *Nature Reviews Molecular Cell Biology* 13 (3): 168–82. http://dx.doi.org/10.1038/nrm3286.

Davis, Lloyd, and Sebastian Greiss. 2018. "Genetic Encoding of Unnatural Amino Acids in *C. elegans*." *Methods in Molecular Biology* 1728: 389–408. https://doi.org/10.1007/978-1-4939-7574-7_24.

Gautier, Arnaud, Duy P Nguyen, Hrvoje Lusic, Wenlin An, Alexander Deiters, and Jason W Chin. 2010. "Genetically Encoded Photocontrol of Protein Localization in Mammalian Cells." *Journal of the American Chemical Society* 132 (12): 4086–88. https://doi.org/10.1021/ja910688s.

Gibb, B, K Gupta, K Ghosh, R Sharp, J Chen, and G D van Duyne. 2010. "Requirements for Catalysis in the Cre Recombinase Active Site." *Nucleic*

Acids Research 38 (17): 5817–32. http://www.nar.oxfordjournals.org/cgi/doi/10.1093/nar/gkq384.

Greiss, Sebastian, and J.W. Jason W Chin. 2011. "Expanding the Genetic Code of an Animal." *Journal of the American Chemical Society* 133 (36): 14196–99. https://doi.org/10.1021/ja2054034.

Guo, F, D N Gopaul, and G D van Duyne. 1997. "Structure of Cre Recombinase Complexed with DNA in a Site-Specific Recombination Synapse." *Nature* 389 (6646): 40–46.

Hobert, Oliver, Robert J Johnston, and Sarah Chang. 2002. "Left-Right Asymmetry in the Nervous System: The *Caenorhabditis elegans* Model." *Nature Reviews. Neuroscience* 3 (8): 629–40.

Kawano, Fuun, Risako Okazaki, Masayuki Yazawa, and Moritoshi Sato. 2016. "A Photoactivatable Cre-LoxP Recombination System for Optogenetic Genome Engineering." *Nature Chemical Biology* 12 (12): 1059–64. https://doi.org/10.1038/nchembio.2205.

Kocabas, Askin, Ching-Han Shen, Zengcai V Guo, and Sharad Ramanathan. 2012. "Controlling Interneuron Activity in *Caenorhabditis elegans* to Evoke Chemotactic Behaviour." *Nature*, September, 1–6. http://dx.doi.org/10.1038/nature11431.

Lang, Kathrin, and Jason W Chin. 2014. "Cellular Incorporation of Unnatural Amino Acids and Bioorthogonal Labeling of Proteins." *Chemical Reviews* 114 (9): 4764–4806. http://pubs.acs.org/doi/abs/10.1021/cr400355w.

Le, Y, S Gagneten, D Tombaccini, B Bethke, and B Sauer. 1999. "Nuclear Targeting Determinants of the Phage P1 Cre DNA Recombinase." *Nucleic Acids Research* 27 (24): 4703–9.

Leifer, Andrew M., Christopher Fang-Yen, Marc Gershow, Mark J. Alkema, and Aravinthan D T Samuel. 2011. "Optogenetic Manipulation of Neural Activity in Freely Moving *Caenorhabditis elegans*." *Nature Methods* 8 (2): 147–52. https://doi.org/10.1038/nmeth.1554.

Luo, J, E Arbely, J Zhang, C Chou, R Uprety, J W Chin, and A Deiters. 2016. "Genetically Encoded Optical Activation of DNA Recombination in Human Cells." *Chemical Communications* 52 (June): 8529–32. http://dx.doi.org/10.1039/C6CC03934K.

Lyssenko, Nicholas N, Wendy Hanna-Rose, and Robert A Schlegel. 2007. "Cognate Putative Nuclear Localization Signal Effects Strong Nuclear Localization of a GFP Reporter and Facilitates Gene Expression Studies in *Caenorhabditis elegans*." *BioTechniques* 43 (5): 560,596,598.

Macosko, Evan Z, Navin Pokala, Evan H Feinberg, Sreekanth H Chalasani, Rebecca A Butcher, Jon Clardy, and C Bargmann. 2009. "A Hub-and-Spoke Circuit Drives Pheromone Attraction and Social Behaviour in *C. elegans*." *Nature* 458 (7242): 1171–75. http://www.nature.com/doifinder/10.1038/nature07886.

Maricq, Andres V., Erin Peckol, Monica Driscoll, and Cornelia I. Bargmann. 1995. "Mechanosensory Signalling in *C. elegans* Mediated by the GLR-1 Glutamate Receptor." *Nature* 378 (6552): 78–81. https://doi.org/10.1038/378078a0.

Maywood, Elizabeth S., Thomas S. Elliott, Andrew P. Patton, Toke P. Krogager, Johanna E. Chesham, Russell J. Ernst, Václav Beránek, Marco Brancaccio, Jason W. Chin, and Michael H. Hastings. 2018. "Translational Switching of Cry1 Protein Expression Confers Reversible Control of Circadian Behavior in

Arrhythmic Cry-Deficient Mice." *Proceedings of the National Academy of Sciences of the United States of America* 115 (52): E12388–97. https://doi.org/10.1073/pnas.1811438115.

Mitani, S, H Du, D Hall, M Driscoll, and M Chalfie. 1993. "Combinatorial Control of Touch Receptor Neuron Expression in *Caenorhabditis elegans*." *Development (Cambridge, England)* 119 (3): 773–83.

Nguyen, Tuan Anh, Marko Cigler, and Kathrin Lang. 2018. "Expanding the Genetic Code to Study Protein–Protein Interactions." *Angewandte Chemie - International Edition* 57 (44): 14350–61. https://doi.org/10.1002/anie.201805869.

Nikić, Ivana, Gemma Estrada Girona, Jun Hee Kang, Giulia Paci, Sofya Mikhaleva, Christine Koehler, Nataliia V Shymanska, Camilla Ventura Santos, Daniel Spitz, and Edward A Lemke. 2016. "Debugging Eukaryotic Genetic Code Expansion for Site-Specific Click-PAINT Super-Resolution Microscopy." *Angewandte Chemie International Edition* 55 (52): 16172–76.

Parrish, Angela R, Xingyu She, Zheng Xiang, Irene Coin, Zhouxin Shen, Steven P Briggs, Andrew Dillin, and Lei Wang. 2012. "Expanding the Genetic Code of *Caenorhabditis elegans* Using Bacterial Aminoacyl-tRNA Synthetase/tRNA Pairs." *ACS Chemical Biology*, May, 120511150716009. http://pubs.acs.org/doi/abs/10.1021/cb200542j.

Radman, Inja, Sebastian Greiss, and J.W. Jason W Chin. 2013. "Efficient and Rapid *C. elegans* Transgenesis by Bombardment and Hygromycin B Selection." *PLoS ONE* 8 (10): e76019. https://doi.org/10.1371/journal.pone.0076019.

Schild, Lisa C., and Dominique A. Glauser. 2015. "Dual Color Neural Activation and Behavior Control with Chrimson and CoChR in *Caenorhabditis elegans*." *Genetics* 200 (4): 1029–34. https://doi.org/10.1534/genetics.115.177956.

Schindler, Suzanne E, Jordan G McCall, Ping Yan, Krzystof L Hyrc, Mingjie Li, Chandra L Tucker, Jin-Moo Lee, Michael R Bruchas, and Marc I Diamond. 2015. "Photo-Activatable Cre Recombinase Regulates Gene Expression in Vivo." *Scientific Reports*, August, 1–8. http://dx.doi.org/10.1038/srep13627.

Schultheis, Christian, Martin Brauner, Jana F Liewald, and Alexander Gottschalk. 2011. "Optogenetic Analysis of GABAB Receptor Signaling in *Caenorhabditis elegans* Motor Neurons." *Journal of Neurophysiology* 106 (2): 817–27. http://jn.physiology.org/cgi/doi/10.1152/jn.00578.2010.

Serfling, Robert, Christian Lorenz, Maja Etzel, Gerda Schicht, Thore Böttke, Mario Mörl, and Irene Coin. 2018. "Designer tRNAs for Efficient Incorporation of Non-Canonical Amino Acids by the Pyrrolysine System in Mammalian Cells." *Nucleic Acids Research* 46 (1): 1–10. https://doi.org/10.1093/nar/gkx1156.

Stiernagle, Theresa. 2006. "Maintenance of *C. elegans*." *WormBook*, January, 1–11. https://doi.org/10.1895/wormbook.1.101.1.

Stirman, Jeffrey N, Matthew M Crane, Steven J Husson, Sebastian Wabnig, Christian Schultheis, Alexander Gottschalk, and Hang Lu. 2011. "Real-Time Multimodal Optical Control of Neurons and Muscles in Freely Behaving *Caenorhabditis elegans*." *Nature Methods* 8 (2): 153–58. http://www.nature.com/doifinder/10.1038/nmeth.1555.

Suzuki, Hiroshi, Tod R Thiele, Serge Faumont, Marina Ezcurra, Shawn R Lockery, and William R Schafer. 2008. "Functional Asymmetry in *Caenorhabditis elegans* Taste Neurons and Its Computational Role in Chemotaxis." *Nature* 454 (7200):

114–17. http://www.nature.com/doifinder/10.1038/nature06927.
Troemel, Emily R., Alvaro Sagasti, and Cornelia I. Bargmann. 1999. “Lateral Signaling Mediated by Axon Contact and Calcium Entry Regulates Asymmetric Odorant Receptor Expression in *C. elegans*.” *Cell* 99 (4): 387–98. https://doi.org/10.1016/S0092-8674(00)81525-1.
Wan, Wei, Jeffery M Tharp, and Wenshe R Liu. 2014. “Pyrrolysyl-tRNA Synthetase: An Ordinary Enzyme but an Outstanding Genetic Code Expansion Tool.” *Biochimica et Biophysica Acta* 1844 (6): 1059–70.
Wes, P. D., and C. I. Bargmann. 2001. “*C. elegans* Odour Discrimination Requires Asymmetric Diversity in Olfactory Neurons.” *Nature* 410 (6829): 698–701. https://doi.org/10.1038/35070581.
White, J G, E Southgate, J N Thomson, and S Brenner. 1986. “The Structure of the Nervous System of the Nematode *Caenorhabditis elegans*.” *Philosophical Transactions of the Royal Society of London. Series B, Biological Sciences* 314 (1165): 1–340.
Wicks, S. R., and C. H. Rankin. 1995. “Integration of Mechanosensory Stimuli in *Caenorhabditis elegans*.” *Journal of Neuroscience* 15 (3 II): 2434–44. https://doi.org/10.1523/jneurosci.15-03-02434.1995.
Yochem, J, T Gu, and M Han. 1998. “A New Marker for Mosaic Analysis in *Caenorhabditis elegans* Indicates a Fusion between Hyp6 and Hyp7, Two Major Components of the Hypodermis.” *Genetics* 149 (3): 1323–34.
Young, Douglas D., and Peter G. Schultz. 2018. “Playing with the Molecules of Life.” *ACS Chemical Biology* 13 (4): 854–70. https://doi.org/10.1021/acschembio.7b00974.
Yumerefendi, Hayretin, Daniel J Dickinson, Hui Wang, Seth P Zimmerman, James E Bear, Bob Goldstein, Klaus Hahn, and Brian Kuhlman. 2015. “Control of Protein Activity and Cell Fate Specification via Light-Mediated Nuclear Translocation.” Edited by Alexander F Palazzo. *PLoS ONE* 10 (6): e0128443-19. http://dx.plos.org/10.1371/journal.pone.0128443.
Zhang, Gong, Siqi Zheng, Haiping Liu, and Peng R. Chen. 2015. “Illuminating Biological Processes through Site-Specific Protein Labeling.” *Chemical Society Reviews* 44 (11): 3405–17. https://doi.org/10.1039/c4cs00393d.

Figure 1

A

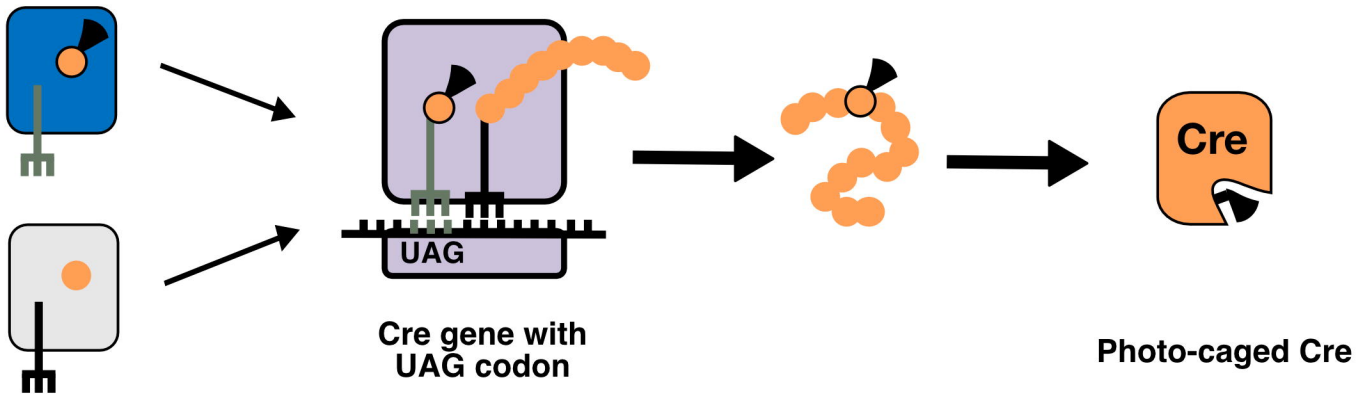
UAG
Cre
Cre gene with
UAG codon
Photo-caged Cre

B

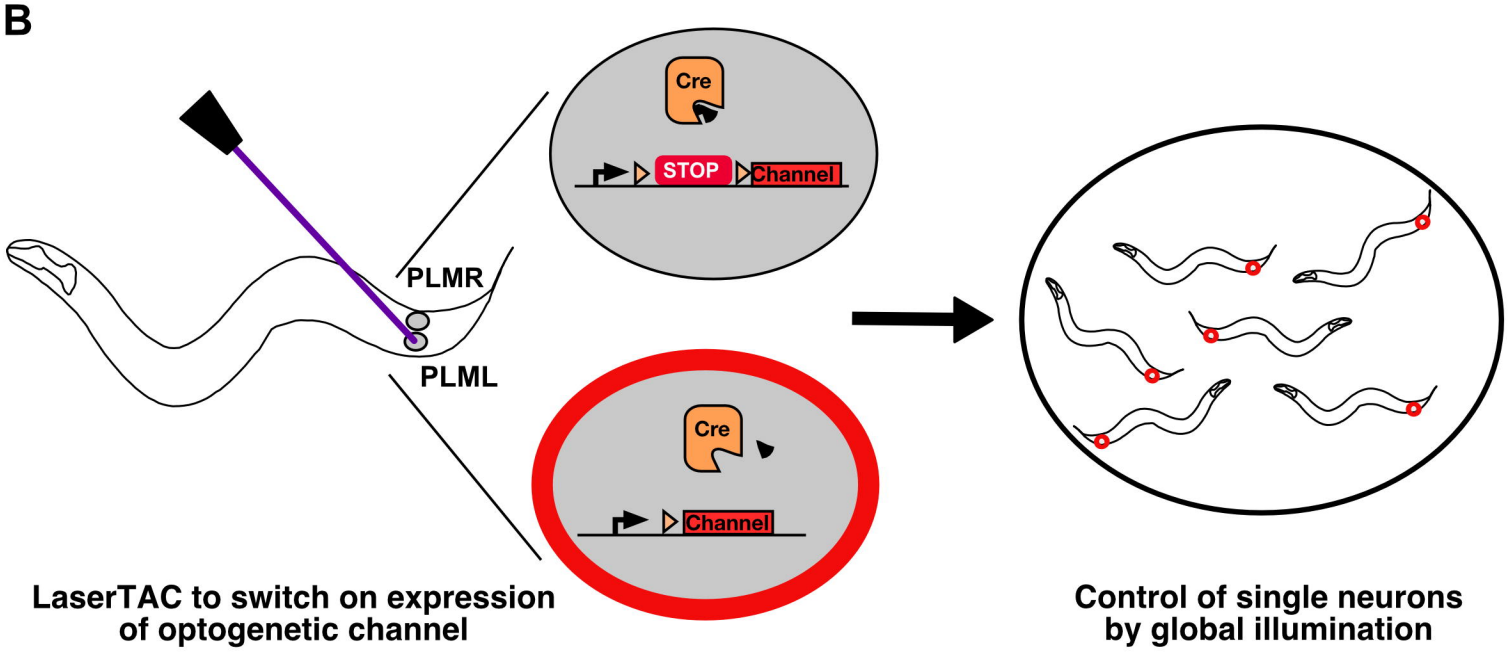
Cre
STOP
Channel
PLMR
PLML
Cre
Channel
LaserTAC to switch on expression
of optogenetic channel
Control of single neurons
by global illumination

Figure 2

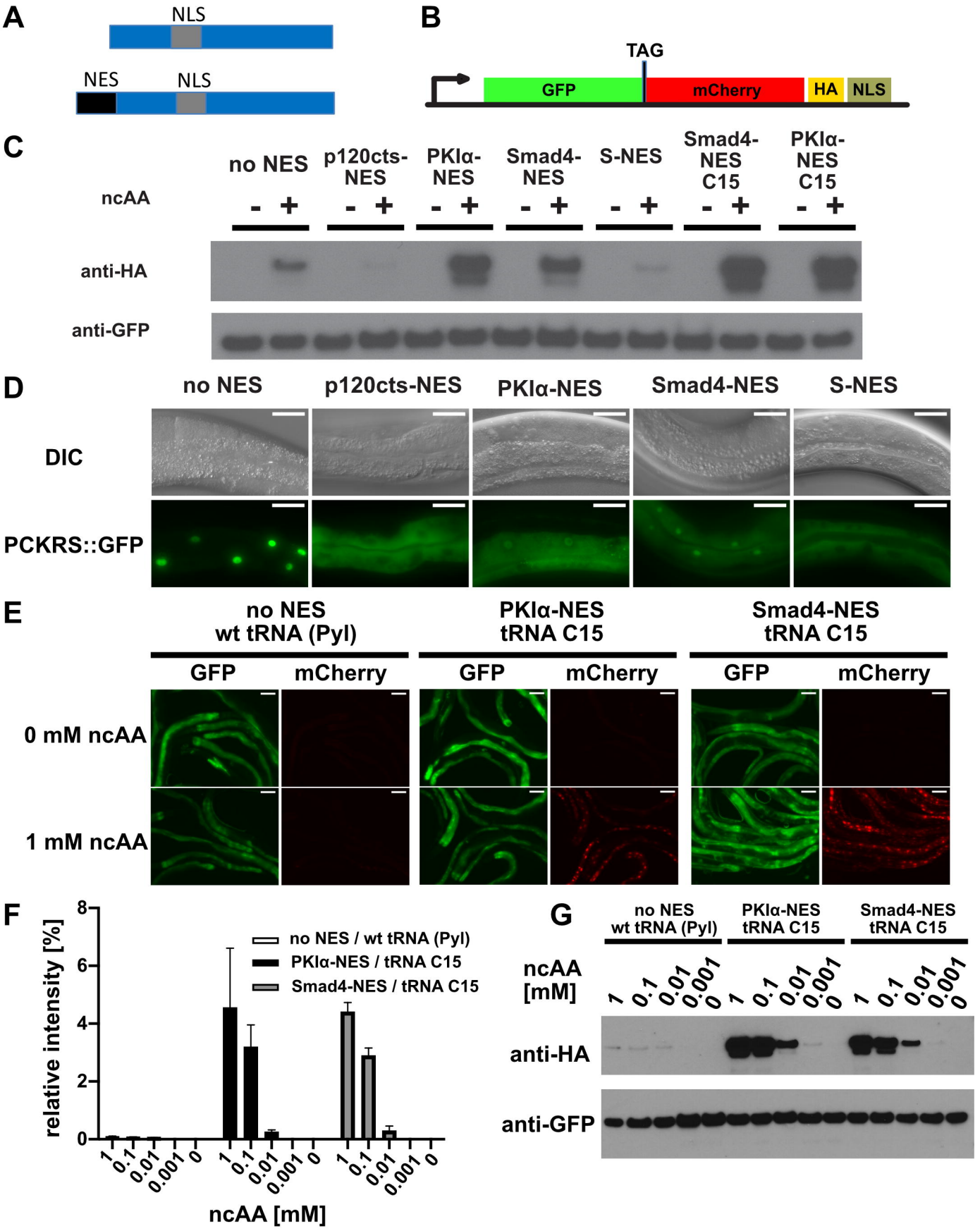
A
NLS
NES
NLS
B
TAG
GFP
mCherry
HA
NLS
C
ncAA
no NES
p120cts-NES
PKIα-NES
Smad4-NES
S-NES
Smad4-NES C15
PKIα-NES C15
- +
anti-HA
anti-GFP
D
no NES
p120cts-NES
PKIα-NES
Smad4-NES
S-NES
DIC
PCKRS::GFP
E
no NES wt tRNA (Pyl)
PKIα-NES tRNA C15
Smad4-NES tRNA C15
GFP
mCherry
0 mM ncAA
1 mM ncAA
F
relative intensity [%]
no NES / wt tRNA (Pyl)
PKIα-NES / tRNA C15
Smad4-NES / tRNA C15
ncAA [mM]
G
no NES wt tRNA (Pyl)
PKIα-NES tRNA C15
Smad4-NES tRNA C15
ncAA [mM]
anti-HA
anti-GFP

Figure 3

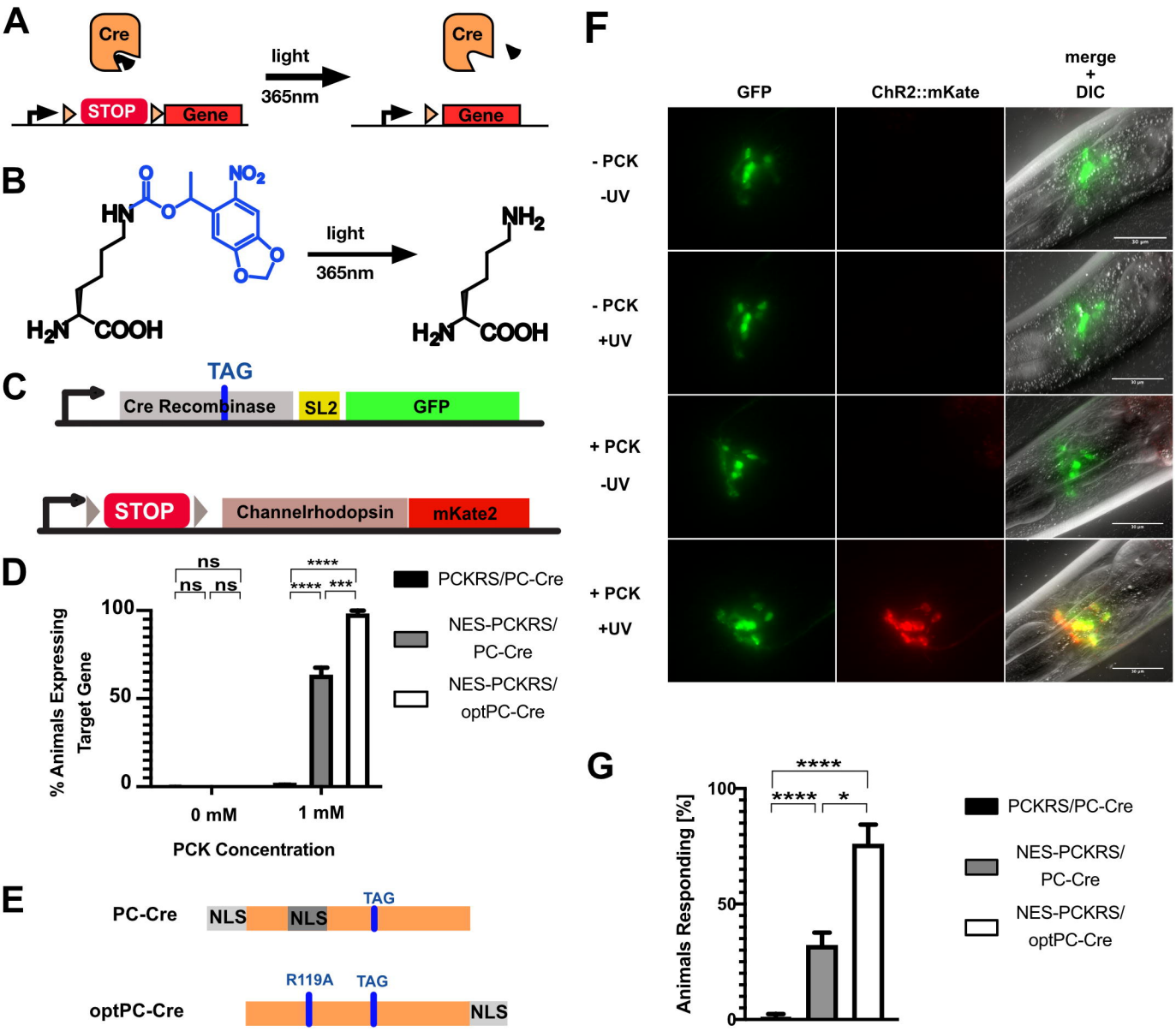
A
Cre
STOP
Gene
light
365nm
Cre
Gene
B
HN
O
O
NO2
O
O
H2N
COOH
light
365nm
NH2
H2N
COOH
C
TAG
Cre Recombinase
SL2
GFP
STOP
Channelrhodopsin
mKate2
D
ns
ns
ns
****
****
***
100
50
0
% Animals Expressing Target Gene
0 mM
1 mM
PCK Concentration
PCKRS/PC-Cre
NES-PCKRS/ PC-Cre
NES-PCKRS/ optPC-Cre
E
PC-Cre
NLS
NLS
TAG
R119A
TAG
optPC-Cre
NLS
F
GFP
ChR2::mKate
merge + DIC
- PCK -UV
- PCK +UV
+ PCK -UV
+ PCK +UV
G
****
****
*
100
50
0
Animals Responding [%]
PCKRS/PC-Cre
NES-PCKRS/ PC-Cre
NES-PCKRS/ optPC-Cre

Figure 4

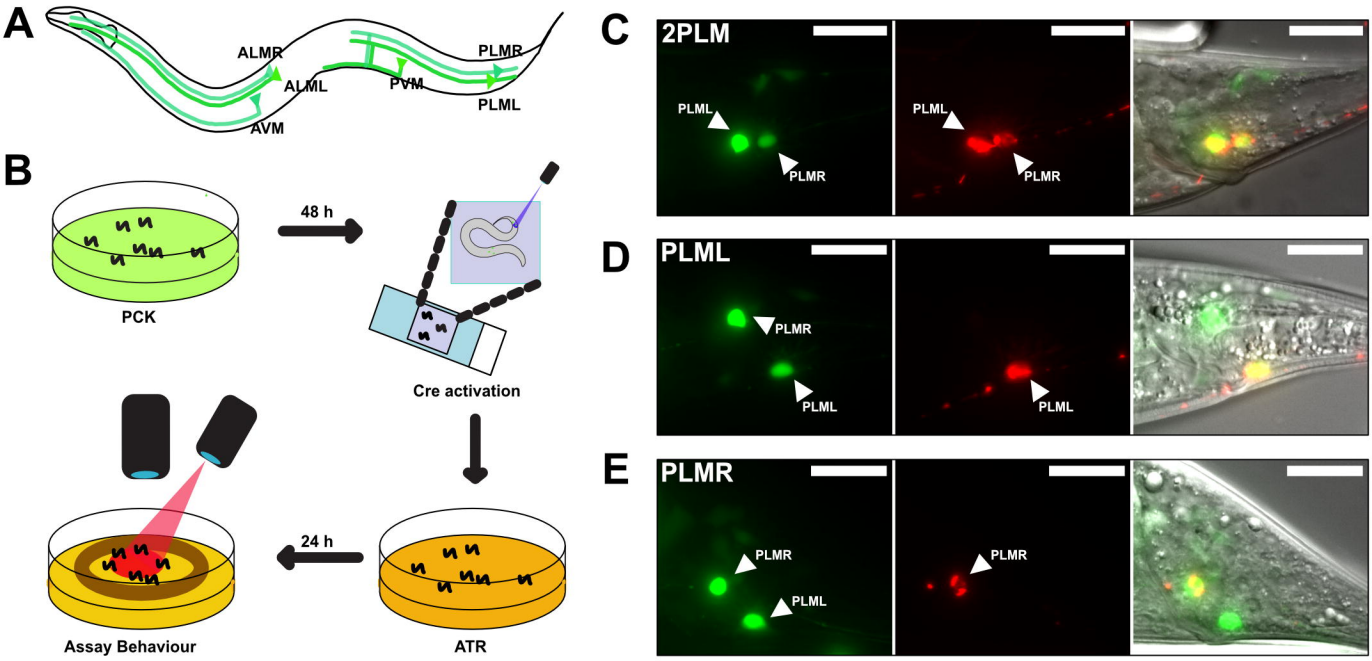
A
ALMR
ALML
AVM
PVM
PLMR
PLML
B
PCK
48 h
Cre activation
ATR
24 h
Assay Behaviour
C
2PLM
PLML
PLMR
D
PLML
PLMR
PLML
E
PLMR
PLMR
PLML

Figure 5

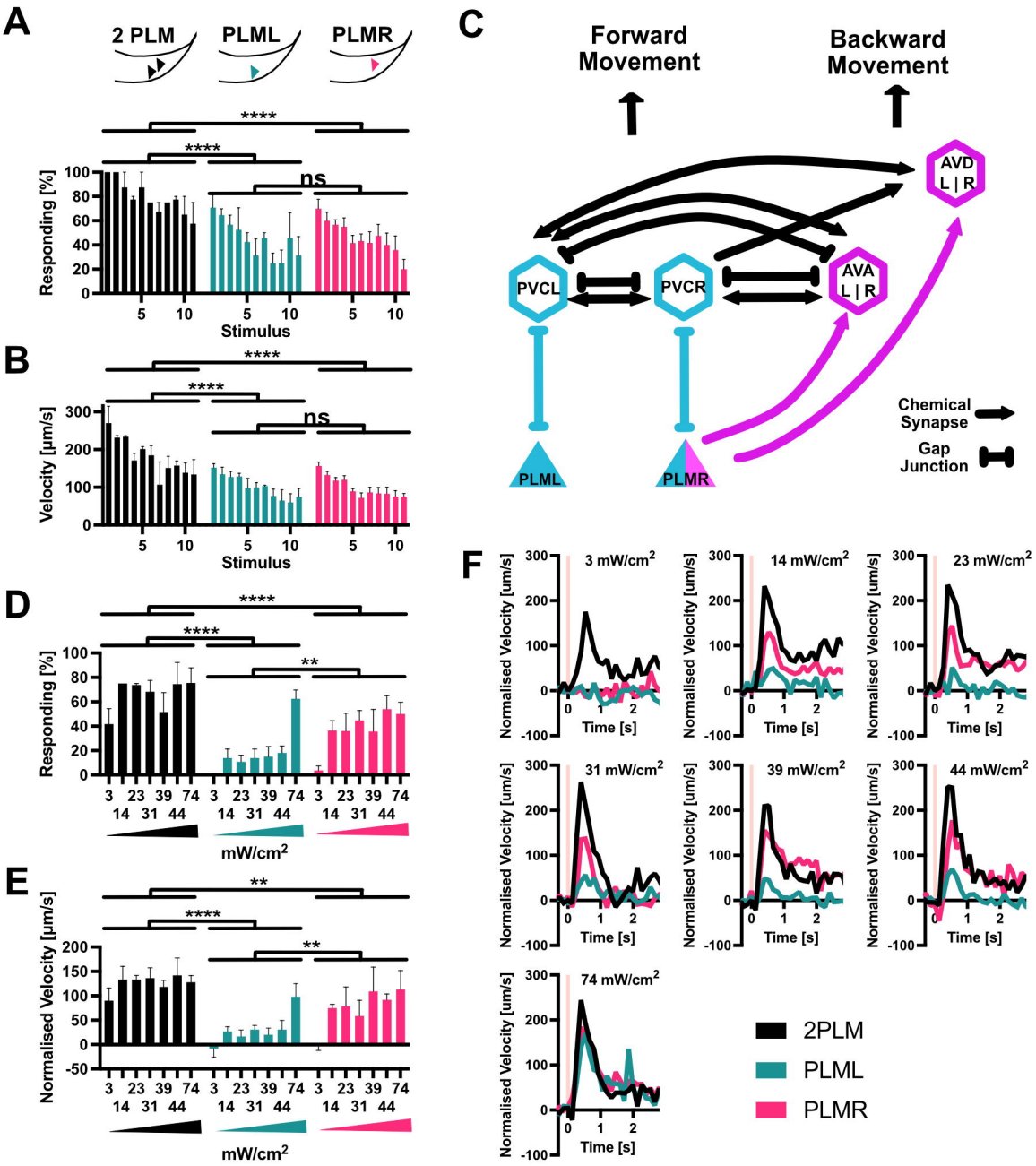
A
2 PLM
PLML
PLMR
****
****
ns
Responding [%]
Stimulus
B
****
****
ns
Velocity [µm/s]
Stimulus
C
Forward Movement
Backward Movement
AVD L | R
PVCL
PVCR
AVA L | R
PLML
PLMR
Chemical Synapse
Gap Junction
D
****
****
**
Responding [%]
mW/cm²
E
**
****
**
Normalised Velocity [µm/s]
mW/cm²
F
3 mW/cm²
14 mW/cm²
23 mW/cm²
31 mW/cm²
39 mW/cm²
44 mW/cm²
74 mW/cm²
Normalised Velocity [um/s]
Time [s]
2PLM
PLML
PLMR